


Janus-Yarn Fabric for Dual-Mode Radiative Heat Management

Muluneh G. Abebe[✉],* Alice De Corte, Gilles Rosolen, and Bjorn Maes

Micro- and Nanophotonic Materials Group, Research Institute for Materials Science and Engineering, University of Mons, 20 Place du Parc, Mons B-7000, Belgium

 (Received 6 July 2021; revised 14 September 2021; accepted 16 September 2021; published 5 November 2021)

Radiative heat management for personal comfort using photonic engineered textiles has the potential to provide a substantial advantage for an energy-efficient and sustainable society. Here, we propose a Janus-yarn design approach for a dual-mode double-sided thermoregulating fabric: a passive-radiative-management textile using asymmetric yarn composition, leading to dual-emissivity characteristics. The fabric provides both passive cooling and heating functions, achieved by wearing the textile inside out. The very strong emissivity contrast is achieved by utilizing both metallic and dielectric fibers within the yarn, benefiting from the plasmonic gap on the one hand and Fabry-Perot and multipole localized modes on the other. This tailored combination of reflective and absorptive structures leads to a substantial emissivity asymmetry between the two surfaces of the fabric ($\Delta\varepsilon = 0.72$). Consequently, the fabric provides a very wide 13.1°C set-point temperature window, with the wearer staying comfortable between 11.3 and 24.4°C.

DOI: [10.1103/PhysRevApplied.16.054013](https://doi.org/10.1103/PhysRevApplied.16.054013)

I. INTRODUCTION

To keep up with the rapidly expanding gap between clean energy production and overall energy demand, optimizing the consumption becomes a necessity. From the various major energy-loss channels, heating and cooling of mostly empty spaces in buildings stands out [1,2]. Therefore, instead of large-scale energy-demanding systems, passive personal thermal management can become a critical measure to lower consumption and guarantee a sustainable future.

For personal thermal-management technologies, more specifically for textiles, controlling the radiative heat transfer has gained more attention than the other mechanisms, due to its universality and high tunability. To a large extent, the human body loses its metabolically generated heat by emitting infrared (IR) radiation centered near 10 μm [3]. Specifically, in an indoor setting such as an office, more than 50% of the heat loss is attributed to IR radiation.

Several state-of-the-art membranes, fibers, and nano- or microparticle-based fabrics have been designed and fabricated for passive (requiring no energy input), single-mode (cooling or heating), and dual-mode (both heating and cooling) thermal-management textiles [4–24]. These designs often rely on photonic designs to control and manipulate radiative transfer from the human body to the ambient. The most attractive thermal-management fabrics are those that provide a dual functionality, as they possess

both cooling and heating modes and switch between modes without external energy input [25–28].

The radiative characteristics of any fabric depend on absorptance, transmittance, and reflectance (which sum to unity). Furthermore, Kirchhoff's law states that at thermodynamic equilibrium, the absorptance equals the emissivity. Fundamentally, in order to cool (heat) the human body, there are two options. One can highly promote (suppress) the transmission of radiation directly through the fabric to the ambient, by designing a transparent (reflective) fabric [e.g., infrared transparent visible opaque fabric (ITVOF) and dynamic transmittance switch textile (DTST)] [4,28]. Alternatively, one can substantially increase (decrease) the radiative emission from the fabric to the ambient, by designing a high- (low-) outer-surface-emissivity textile [26].

Recently, Janus-membrane fabrics have been reported with asymmetric radiative properties, due to both low- and high-emissivity materials [29–35]. However, unlike fabrics made out of fibers and yarns, membrane-based technologies often lack air and moisture permeability to provide the required thermal comfort, so other technologies should be developed.

In this work, we demonstrate a promising Janus-yarn framework for a personal thermoregulating fabric. The passive fabric is composed of a staggered asymmetric structure, which controls the radiative transfer from the human body to the ambient by strongly modulating the emissivity. We perform a comprehensive numerical study of the optical and thermal properties of the design to determine optimized parameters for both heating and

*Corresponding author. mulunehgeremew.abebe@umons.ac.be

cooling functionalities. The switching between the cooling and the heating mode is achieved through physical flipping of the fabric. The design capitalizes on numerous photonic effects that stem from the design geometry and material choice, as both metallic and dielectric materials are present. The photonic and thermal properties lead to a substantial emissivity contrast ($\Delta\varepsilon = 0.72$) between the two surfaces of the fabric, providing the two modes of operation. Consequently, this leads to a very significant 13.1°C set-point temperature window for comfort.

In Sec. II, we explain in detail the working principle of the Janus-yarn textile. In Sec. III, we present both modeling schemes: the electromagnetic (Sec. III A) and the thermal approach (Sec. III B). In Sec. IV, we assess the modeling results and evaluate the design performance and Sec. V concludes.

II. PROBLEM STATEMENT AND DESIGN PRINCIPLE

Traditional textiles can only be utilized comfortably in a limited temperature window, functioning only in one mode (cooling or heating), even under dynamic ambient temperature changes. In a cold environment, where the ambient temperature is below the natural comfort zone, one must use fabrics designed for warming purposes, such as winter garments, or increase the number of layers of clothing. On the other hand, in a hot environment, when the ambient temperature is above the natural comfort zone, clothing that relieves heat stress from the human body is necessary.

However, when the ambient temperature changes, traditional fabrics fail to accommodate both cooling and heating functionalities. Due to temperature fluctuations, which have become more common in recent years, addressing the lack of flexibility in single-mode textiles is an important challenge, potentially leading to fewer health problems. However, single-mode fabrics push the temperature window only in a single direction. In contrast, our design for a Janus-yarn fabric possesses dual-mode functionality, with a static switching capability (via inversion of

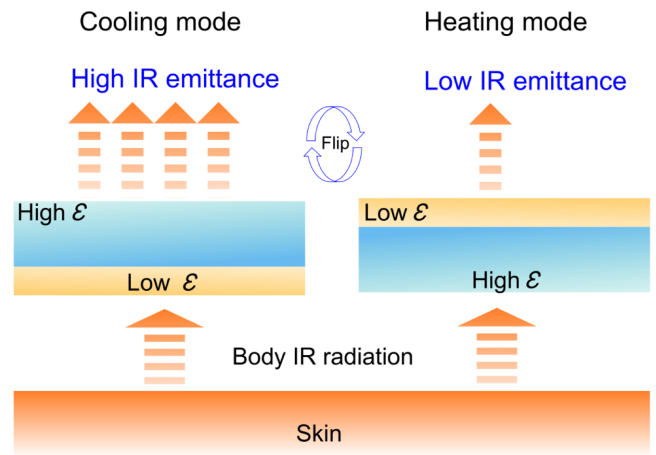


FIG. 1. The working principle of emissive Janus-based textile. When a high-emissivity layer faces the ambient, the fabric is in cooling mode (left). Once the textile is flipped and the low-emissivity layer faces outside, the fabric is in heating mode (right).

the fabric). This provides an opportunity to thermoregulate for a large ambient temperature variation, consequently resolving both traditional and single-mode textile flexibility issues.

The core principle relies on the outer-surface emissivity of the fabric. This stems from the Stefan-Boltzmann radiative-emission law, which states that the total power radiated from an object with a surface area S , temperature T , and emissivity ε is $P = S\varepsilon\sigma T^4$, where σ is the Stefan-Boltzmann constant. Changing this emissivity from low to high strongly modulates the radiative heat transfer to the ambient (see Fig. 1). Therefore, for cooling functionality, the high-emissivity layer of the fabric faces the ambient such that the surface acts as an infrared radiator. On the other hand, flipping the same fabric exposes the low-emissivity side to the ambient, acting as radiative insulation. Further, because the fabric is constituted out of yarns, which are bundles of fibers, it provides the required

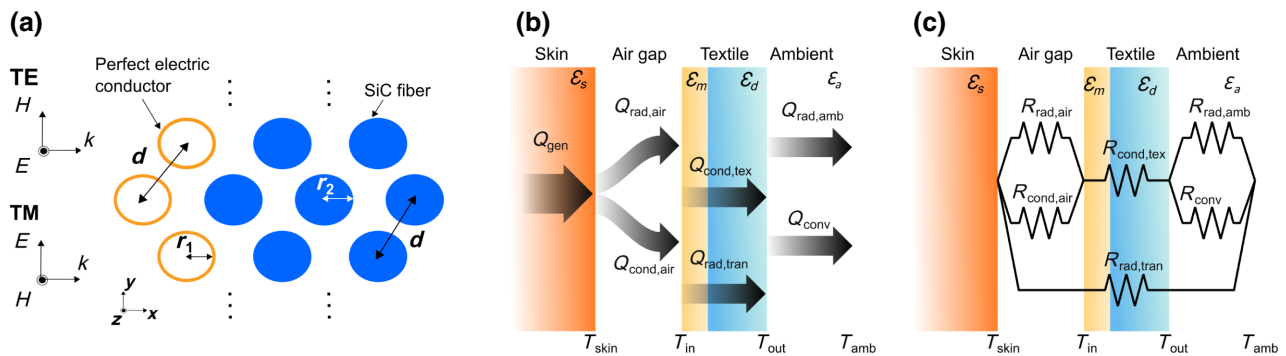


FIG. 2. (a) The simulation model, with the polarization convention and incidence direction. The pattern is repeated in the vertical y direction. (b) The main heat-flow channels when the fabric covers skin, with an air gap in between. (c) The thermal-circuit analogy.

air permeability, water-vapor transmission, and moisture-wicking properties for standard thermal comfort [36,37].

The asymmetric emissivity of the fabric is achieved from the photonic structure of the Janus yarns, which use two different materials: highly absorbing or highly emitting dielectric microfibers and highly reflecting non-absorbing or emitting metallic microfibers [Fig. 2(a)]. Both dielectric and metallic fibers are staggered in a specific photonic geometry to provide the optimal Janus functionality. Consequently, for the heating (cooling) mode, the metal (dielectric) side of the yarn faces the ambient, as discussed further on.

III. MODELING APPROACH

The proposed Janus-yarn textile provides comfort over a large temperature range (called the set-point temperature window) when the design parameters are optimized. To determine this temperature window, first we utilize an electromagnetic model (Sec. III A) to retrieve the spectral and total radiative parameters and consequently we feed these characteristics into the thermal model (Sec. III B).

A. Electromagnetic model

To study the IR radiative response of the design, we utilize a commercial finite-element-based Maxwell's equations solver (COMSOL Multiphysics). The geometry is constituted from metallic fibers with radius r_1 on one side and dielectric fibers with radius r_2 on the other [Fig. 2(a)], all in a hexagonal pattern with center-to-center distance d . The perfect electric conductor (PEC) boundary condition is used around the metal fibers. Consequently, perfect reflection without any material loss is achieved from these surfaces, which is a very good approximation for many metals in the relevant IR wavelength range [28].

Due to its strong IR-absorbing property in the relevant wavelength region (4–25 μm), silicon carbide (SiC) is used as the dielectric fiber material, with refractive indices derived from Ref. [38] (see Fig. 1 in the Supplemental Material [39]). However, other materials with significant IR absorption (such as cellulose and polydimethylsiloxane) could be employed accordingly, by taking factors such as size, mechanical flexibility, manufacturing techniques, and so on into consideration [34,40–42].

Simulations are performed with perpendicular incidence (for TE- and TM-mode polarization) from both sides: (1) the metallic side [on the left in Fig. 2(a)] and (2) the dielectric side [on the right in Fig. 2(a)]. Floquet periodic boundary conditions are used on the top and bottom to represent an infinite repetition in the vertical direction [see Fig. 2(a)] and the different diffraction orders are included using port conditions on the right and left sides. Due to computation time and resources, the geometric optimization is done using two-dimensional (2D)

simulations. However, as discussed later on, full three-dimensional (3D) simulations are deployed to validate the 2D results and for the best-performing designs.

For the thermal model, one needs the total radiative quantities: transmittance (τ), absorptance ($\alpha = \varepsilon$), and reflectance (ρ). These are the spectrally integrated transmission T , reflection R , and absorption A , weighted with the human-body emissivity, for which we employ the Planck distribution (ϕ_{bb}) with a skin temperature of 34°C:

$$\tau/\alpha/\rho = \frac{\int_{\lambda_1}^{\lambda_2} T/A/R(\lambda)\phi_{\text{bb}}(\lambda)d\lambda}{\int_{\lambda_1}^{\lambda_2} \phi_{\text{bb}}(\lambda)d\lambda}, \quad (1)$$

with the wavelength range from $\lambda_1 = 4 \mu\text{m}$ to $\lambda_2 = 25 \mu\text{m}$, containing most of the human-body radiation.

B. Thermal model

The cooling and heating performance is assessed with the ambient set-point temperature, which is determined from a heat-transfer analysis using thermal-circuit models (see the details in the Supplemental Material [39]). We treat the thermal dissipation from the human body to the ambient as a one-dimensional steady-state heat-transfer problem in dry conditions, hence ignoring mass transfer through the fabric. The three heat-transfer channels, when the fabric covers the skin with an air gap in between, are radiation, conduction, and convection [see Fig. 2(b)]. Note that the schematic only presents the cooling model: the dielectric side (ε_d) faces the ambient, the metallic side (ε_m) faces the skin.

For a semitransparent (absorbing and emitting) fabric layer, radiative ($Q_{\text{rad,air}}$) and conductive ($Q_{\text{cond,air}}$) heat-transfer processes constitute the exchange through the air gap, while the heat dissipation from the fabric to the ambient is via radiation ($Q_{\text{rad,amb}}$) and convection exchanges ($Q_{\text{rad,conv}}$). Conductive exchange ($Q_{\text{cond,tex}}$) contributes to the heat transfer in the textile. Furthermore, radiation ($Q_{\text{rad,tran}}$) exchange occurs between the skin and the ambient with transmission through the fabric layer. When the transmission through the fabric is low, one can assume an opaque layer, so $Q_{\text{rad,tran}} = 0$ [see Figs. 3(a) and 3(b) in the Supplemental Material [39]]. Note that convective heat transfer in the air gap is negligible, due to the small Rayleigh number, which stems from the relatively small air-gap thickness [43].

The corresponding thermal-circuit model is constructed with thermal resistances [Fig. 2(c)], where T_{skin} and ε_s are the skin temperature and emissivity. T_{amb} and ε_a are the ambient temperature and emissivity. T_{in} is the inner and T_{out} the outer textile surface temperature. $R_{\text{rad,air}}$ (which varies with fabric flipping) and $R_{\text{cond,air}}$ are the radiative and conduction thermal resistances of air. $R_{\text{cond,tex}}$ is the textile conductive thermal resistance, $R_{\text{rad,tran}}$ the thermal resistance of radiative transmission, $R_{\text{rad,amb}}$ (which varies

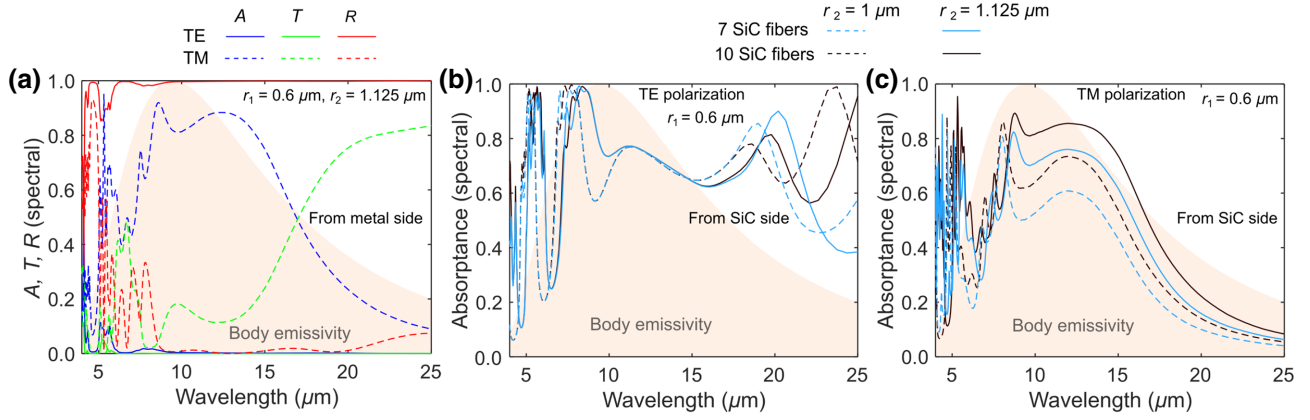


FIG. 3. (a) The TE- and TM-mode absorptance (A), transmittance (T), and reflectance (R) of Janus yarn ($r_1 = 0.6 \mu\text{m}$, $r_2 = 1.125 \mu\text{m}$, $d = 3 \mu\text{m}$) illuminated from the metallic side. (b),(c) The (b) TE- and (c) TM-mode absorptance (A) for fixed r_1 ($0.6 \mu\text{m}$) while varying r_2 (1 and $1.125 \mu\text{m}$) and the number of SiC fibers (7 and 10), with incidence from the dielectric side.

with fabric flipping) is the radiative thermal resistance of ambient, and R_{conv} the convective thermal resistance.

The requirement for a wearer's thermal comfort is the balance between metabolic heat generation (Q_{gen}) and total heat loss in dry condition (Q_{dry}). The total heat loss is controlled by the total thermal resistance R_{tot} between skin and ambient. The total heat flux through the air gap and fabric to the ambient is given by

$$Q_{\text{gen}} = Q_{\text{dry}} = \frac{T_{\text{skin}} - T_{\text{amb}}}{R_{\text{tot}}}. \quad (2)$$

Further necessary thermal constants are detailed in the Supplemental Material [39].

Crucially, due to the asymmetric emissivity characteristics, the Janus fabric possesses two different R_{tot} values for heating and cooling modes, respectively, which we can calculate using the thermal-circuit model. Subsequently, by considering a constant metabolic heat generation of 70 W/m^2 (for a sedentary individual with a skin temperature of 34°C) and with $\varepsilon_{\text{skin}} = 0.98$ and $\varepsilon_{\text{amb}} = 1$, we can determine the cooling and heating set-point temperatures, as discussed later on.

IV. RESULTS AND DISCUSSION

This section presents results from electromagnetic and thermal calculations: the IR response highlighting various photonic properties (Sec. IV A), geometry optimization and 3D-simulation validation (Sec. IV B), and fabric performance analysis using thermal properties (Sec. IV C).

A. Electromagnetic properties

For a given geometry ($r_1 = 0.6 \mu\text{m}$, $r_2 = 1.125 \mu\text{m}$, $d = 3 \mu\text{m}$), the IR response from the metallic side (A , T , R) for the TE mode (solid lines) and the TM mode (dashed lines) are displayed in Fig. 3(a). For the TE mode,

R (solid red line) and T (solid green) show a plasmonic gap stationed above a cutoff around $\lambda = 4 \mu\text{m}$, a fundamental metallic effect that blocks the TE-mode radiation from transmitting to the dielectric fibers and through the yarn [28,44–48]. As a result, there is a close-to-zero overall TE-mode absorption (solid blue line), leading to a very low emission from the metallic side of the yarn.

However, unlike the TE-mode case, there is no plasmonic gap for TM-mode polarization. Therefore, the TM mode is transmitted through the metallic fibers and a substantial amount is absorbed (dashed blue line) in the dielectric fibers or reaches the ambient (dashed green). Unfortunately, this TM-mode absorption and transmission increases the averaged unpolarized characteristics, which would negatively affect the heating mode operation. However, a crossed configuration of the metallic fibers [see inset of Fig. 5(a)] benefits both polarizations, which drastically cuts the unpolarized transmission and absorption.

The crossed-metal-wire configuration works as follows: the TE-mode orientation for the first array behaves as the TM mode for the second (90° rotated) array and vice versa [see the inset of Fig. 5(a)]. Subsequently, there is always an array with an electric field parallel to the wire, leading to a strong reflection on one of the arrays due to the plasmonic gap [see Figs. 2(a) and 2(b) in the Supplemental Material [39]]. Accordingly, the total emissivity from the metal side with crossed wires is very close to the spectrally integrated value for the TE mode in the 2D situation (without crossed wires), which is validated with 3D simulations, at about $\varepsilon_m = 0.017$, guaranteeing a very low emissivity from the metallic side and allowing a heating mode.

Most of the TE-mode and TM-mode radiation impinging from the dielectric side enters the Janus yarn and is substantially absorbed by the dielectric fibers [see Fig. 3(b)]. Radiation that passes the dielectric fibers in the TE mode is reflected by the metallic fibers due to the plasmonic gap

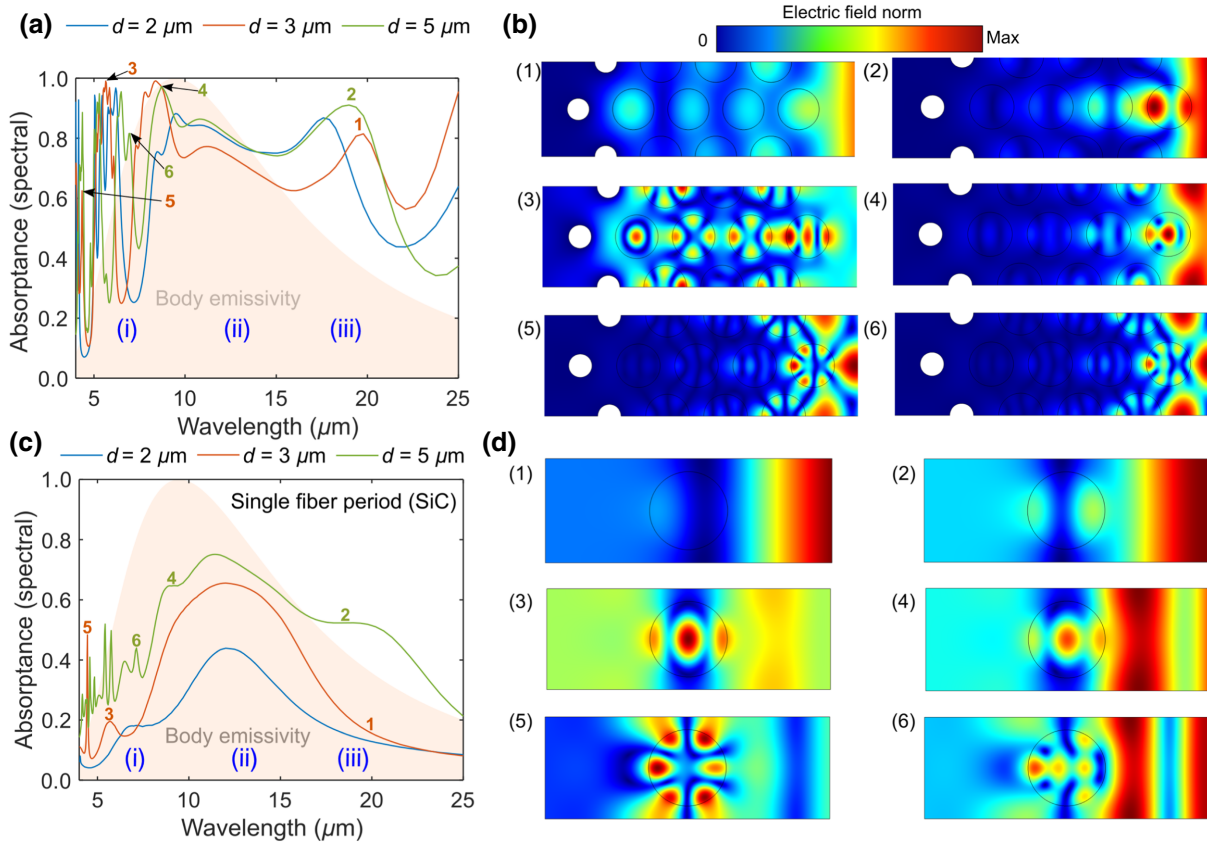


FIG. 4. (a) The TE-mode absorptance of a yarn ($r_2 = 1.125 \mu\text{m}$) for separations d of 2, 3, and $5 \mu\text{m}$, dielectric incidence. (b) The electric field norm at (1) $\lambda = 19.8 \mu\text{m}$, (2) $\lambda = 19 \mu\text{m}$, (3) $\lambda = 5.5 \mu\text{m}$, (4) $\lambda = 8.7 \mu\text{m}$, (5) $\lambda = 4.45 \mu\text{m}$, and (6) $\lambda = 7.13 \mu\text{m}$. (c) The TE-mode absorptance of single-fiber SiC with diameters of 1.5, 2.25, and $3.75 \mu\text{m}$ (with $d = 2, 3, \text{ and } 5 \mu\text{m}$). (d) The electric field norm at (1) $\lambda = 19.8 \mu\text{m}$, (2) $\lambda = 19 \mu\text{m}$, (3) $\lambda = 5.5 \mu\text{m}$, (4) $\lambda = 8.7 \mu\text{m}$, (5) $\lambda = 4.45 \mu\text{m}$, and (6) $\lambda = 7.13 \mu\text{m}$.

(which acts as an IR mirror), enhancing the absorption path length and the emission. On the other hand, the TM-mode radiation that manages to pass the dielectric largely passes the metallic fibers, as the plasmonic gap is absent, which negatively affects the emission. Note that this can again be solved by using the crossed-wire configuration.

In cooling mode, the main design goal is to achieve a high emissivity from the dielectric side; hence, one can optimize the various geometric parameters to increase the absorption: fiber size, separation distance, number of fibers, and so on (see Fig. 4 in the Supplemental Material [39]). To illustrate, we present the absorptance for a fixed fiber-separation distance ($d = 3 \mu\text{m}$) with varying fiber size ($r_2 = 1$ and $1.125 \mu\text{m}$) and number of SiC fibers (seven and ten) [see Figs. 3(b)–3(c)]. The geometry with ten SiC fibers contains three additional fibers to the right of Fig. 2(a) (adding another layer in the hexagonal arrangement).

Under the human-body emissivity curve, for the TE mode [Fig. 3(b)], the absorption contrast between different fiber sizes (solid and dashed lines), as well as between different numbers of fibers (light blue and dark brown) is

small. On the other hand, for the TM mode [Fig. 3(c)], there exists a noticeable contrast: increasing the size and the number of fibers gives better absorption. For example, the best-performing structure is the largest $r_2 = 1.125 \mu\text{m}$ with ten fibers (solid dark brown line), while the least-performing is $r_2 = 1 \mu\text{m}$ with seven fibers (light blue dashed line).

Next, we vary the fiber separation ($d = 2, 3, \text{ and } 5 \mu\text{m}$) for a fixed radius ($r_1 = 0.6 \mu\text{m}$ and $r_2 = 1.125 \mu\text{m}$) and ten dielectric fibers [for the TE-mode absorption, see Fig. 4(a)]. In general, the absorption is high; however, there are variations, originating from various photonic characteristics. One distinguishes three regions: (i) narrow peaks at shorter wavelengths ($4\text{--}9 \mu\text{m}$), (ii) a relatively constant high-absorption plateau at medium wavelengths ($10\text{--}15 \mu\text{m}$), and (iii) broader resonances at longer wavelengths ($16\text{--}25 \mu\text{m}$).

These regimes are interpreted via the field profiles (electric field norm) at specific peaks [see Fig. 4(b)]. Within region (i), panels (3)–(6) show localized higher-order multipole-type resonances, with, e.g., quadrupoles in panel (3) ($d = 3 \mu\text{m}$, $\lambda = 5.5 \mu\text{m}$) and hexapoles in panel (5).

This leads to multiple narrow-band increases of the local field and the absorption. Within region (iii), panel (1) ($d = 3 \mu\text{m}$, $\lambda = 19 \mu\text{m}$) shows globally a Fabry-Perot type mode, with an envelope and multiple maxima. Panel (2) ($d = 3 \mu\text{m}$, $\lambda = 17.6 \mu\text{m}$) develops coupled localized dipolar modes. The latter modes are lower order and thus more broadband. On the other hand, region (ii) is relatively featureless, leading to a plateau of high absorption, which can be understood via the large absorption of SiC in this range (see Fig. 1 in the Supplemental Material [39]).

To obtain a clearer understanding of the multifiber yarn modes, we compare with a single dielectric fiber period of the same size [for the TE-mode absorptance, see Fig. 4(c)], with field profiles in Fig. 4(d). Similar to the yarn, in region (i), the single-fiber spectral curve exhibits narrow peaks (higher-order multipoles); for example, panels (3) ($d = 3 \mu\text{m}$, $\lambda = 5.5 \mu\text{m}$) and (4) ($d = 5 \mu\text{m}$, $\lambda = 8.7 \mu\text{m}$) show trilobal modes [similar to Fig. 4(d) (3) and (4)], whereas panels (5) ($d = 3 \mu\text{m}$, $\lambda = 4.45 \mu\text{m}$) and (6) ($d = 3 \mu\text{m}$, $\lambda = 7.13 \mu\text{m}$) show sextupolelike modes [similar to Fig. 4(d) (5) and (6)]. In region (ii), there exists a broad high-absorption peak, similar to the plateau of the yarn [Fig. 4(a)]. In region (iii), there is a dipolar peak or shoulder for $d = 5 \mu\text{m}$ (panel 2), similar to the dipole observed in the yarn profile [Fig. 4(b) (2)].

However, some absorption peaks from the yarn [region (iii) in Fig. 4(a)] are not present for the single fiber. Furthermore, the single-fiber field for $d = 3 \mu\text{m}$ does not have a particular profile [panel (1)]; thus, the yarn mode [Fig. 4(b) (1)] points to a global Fabry-Perot type mode, with an envelope over the whole structure, which is not possible with the single fiber. Overall, one observes that the interplay of local and global field enhancements aids the achievement of strong absorption or emission via the dielectric fibers.

B. Optimization and 3D validation

With these results, an overall design optimization using 2D simulations (with the crossed-wire approach in mind) indicates the following geometric parameters: three metallic fibers per period ($r_1 = 0.6 \mu\text{m}$, $d = 3 \mu\text{m}$) to sufficiently cut the transmission ($\tau = 0.0035$), leading to a low total emissivity ($\varepsilon_m = 0.017$) for heating performance. The latter combined with ten dielectric fibers ($r_2 = 1.125 \mu\text{m}$, $d = 3 \mu\text{m}$) delivers a large total emissivity ($\varepsilon_d = 0.72$) required for cooling.

To confirm the accuracy of the 2D results and further ground the crossed-wire method, we employ 3D simulations with actual crossed metallic fibers [see the inset in Fig. 5(a)]. The spectral response for unpolarized radiation (averaged polarization) for incidence from the metallic and dielectric side is displayed in Figs. 5(a) and 5(b), respectively. From the metallic side, a very low spectral absorptance and transmittance is achieved [blue and green lines in Fig. 5(a)], leading to a very low total emissivity ($\varepsilon_m = 0.017$) and transmittance ($\tau = 0.0039$). Therefore, crossing the metallic fibers has the expected, very useful, effect of a plasmonic gap for both polarizations. From the dielectric side [Fig. 5(b)], the absorptance is very large: above 0.7 from 8 to 15 μm and almost reaching 1 at a peak around 9 μm , resulting in a high total emissivity ($\varepsilon_d = 0.74$). Finally, the transmittance is very low from both sides, which is important for the thermal properties.

In conclusion, the simulation results using 3D modeling agree with 2D results [see also Figs. 2(c) and 2(d) in the Supplemental Material [39]]. Thus, the crossed-wire approach works very well and can be modeled efficiently via 2D for design optimization.

Furthermore, the operational mechanism of the design is tolerant to moderate amounts of disorder. Fundamentally, if some (or all) of the monofilaments are shifted from their

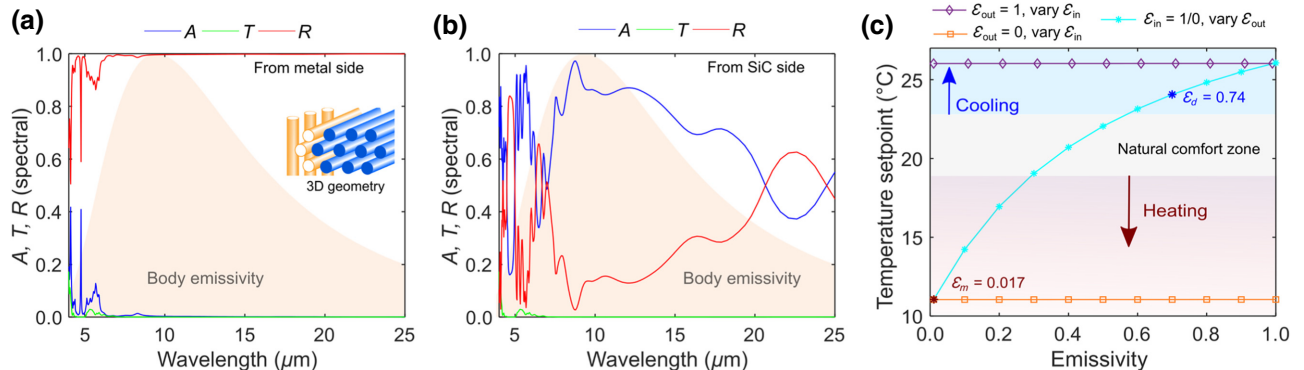


FIG. 5. The unpolarized absorptance, transmittance, and reflectance of a Janus yarn (crossed-wire 3D geometry) for the best parameters (ten SiC fibers, three metallic fibers, $r_1 = 0.6 \mu\text{m}$, $r_2 = 1.125 \mu\text{m}$, $d = 3 \mu\text{m}$). Incidence from the (a) metal and (b) dielectric side. (c) The set points of the ambient temperature for maintaining thermal comfort as a function of the IR emissivity of the textile at the inner surface (ε_{in}) and outer surface (ε_{out}). The natural comfort zone is the region where no heating or cooling is needed; above the natural comfort zone (light blue area), cooling is required, while below the natural comfort zone (light red region), heating is required.

original positions, the crucial photonic effects that drive the operational mechanism (i.e., the plasmonic gap, Fabry-Perot, and multipole localized modes) are weakly affected (see Fig. 6 in the Supplemental Material [39]).

C. Thermal properties

With the thermal model, by considering all thermal parameters [see Table 1 in the Supplemental Material [39]] and assuming a very low (close-to-zero) transmission, we can determine the set-point temperature for a variety of situations [see Fig. 5(c)].

The maximum ideal upper set-point temperature of a cooling fabric is 26°C, which is achieved with $\varepsilon_{\text{out}} = 1$ and the inside emission no longer plays a role (horizontal purple line, which is a function of ε_{in}). The minimum ideal lower set-point temperature of a heating fabric is 11°C, which is reached when $\varepsilon_{\text{out}} = 0$ and the inside emission is again not a factor (horizontal orange line, which is a function of ε_{in}).

However, varying ε_{out} while fixing ε_{in} to one or zero (i.e., both give the same result) results in a wide set-point window [the cyan curve in Fig. 5(c)]. This demonstrates the vital importance of the outer-surface emissivity of a fabric to modulate between upper and lower set-point temperatures, in order to provide thermal comfort in a very-low-transmission situation. The influence of increased transmittance is discussed in detail in Figs. 3(a)–3(c) in the Supplemental Material [39].

Most, if not all, smart fabrics for personal thermal management with very low (close-to-zero) transmission provide thermal comfort within this set-point window. Single-mode fabrics have a single set-point temperature, an upper or a lower bound, depending on their cooling or heating function. Dual-mode fabrics have two set points, which depend on their mode of operation.

A typical set-point temperature band for human thermal comfort in buildings, especially in offices, is subjective and requires polls and statistics; thus we consider a general extended average of 19–23°C natural comfort zone for traditional textiles [the light gray band in Fig. 5(c)].

The proposed Janus-yarn fabric attains a 24.4°C (blue star on cyan curve) upper bound set-point temperature in cooling mode ($\varepsilon_{\text{out}} = \varepsilon_d = 0.74$) and a 11.3°C (dark red star on cyan curve) lower bound in heating mode ($\varepsilon_{\text{out}} = \varepsilon_m = 0.017$). This leads to a very large thermal-comfort temperature window of 13.1°C.

In comparison, the lowest bound is 3°C lower than for the Mylar or space blanket (14.3°C) [49], 2.6°C lower than for the dual-mode textile (13.9°C) in Ref. [26], and 3.4°C lower than for the nanoporous metallized polyethylene textile (14.7°C) in its cotton-polyethylene-Ag configuration [7]. Therefore, the proposed design heating functionality is not only better than typical traditional winter fabrics but also shows superiority over various

advanced thermal-management textiles. Furthermore, the highest bound is 1.6°C larger than that of cotton (22.8°C) and 0.1°C more than for the dual-mode textile (24.3°C) in [26].

Furthermore, the influence of ambient airflow on the performance of the design is investigated by varying the convective heat-transfer coefficient [50]. Subsequently, as one expects, the cooling functionality improves with increasing ambient air circulation, while negatively impacting the heating functionality (see Fig. 7 in the Supplemental Material [39]).

Hence, this design provides a very wide ambient set-point temperature window of 13.1°C. A wide set-point window of 10.4°C for a radiative-emissivity-control fabric design has been reported, which was for a dual-mode approach that also used fabric flipping [26]. Therefore, our Janus-yarn fabric grants an additional 2.7°C window for more flexibility to preserve the thermal comfort of the wearer in dynamic conditions.

V. CONCLUSION

In this work, we numerically demonstrate a Janus yarn configuration, leading to a passive personal-thermoregulation fabric that provides both cooling and heating functionalities. We implement a detailed 2D and 3D electromagnetic and heat-transfer analysis to evaluate the radiative and thermal performance. The fabric exhibits a strongly asymmetric emissivity, due to a tailored choice of materials and geometries, providing an optimized exploitation of photonic effects such as the plasmonic gap and localized resonances. The fabric switches from one mode to the other by mechanical flipping, so that the design achieves a large emissivity contrast of about 0.7 between the two surfaces, leading to a very wide comfort window of 13.1°C.

ACKNOWLEDGMENTS

We acknowledge support from the INTERREG PHOTONITEX project.

Muluneh G. Abebe and Alice De Corte contributed equally to this work.

APPENDIX

For TE-mode polarization, the absorption increases slightly with d . This absorption increase is directly related to the shift of the plasmonic gap from the lower- to the higher-wavelength region when the fiber-separation distance increases. As a result, some electromagnetic radiation reaches the SiC fibers and is absorbed. The plasmonic gap is optimized accordingly using the fiber size and separation distance. For example, Figs. 6(a) and 6(c) show absorptance spectra for (a) TE-mode and (b) TM-mode-polarization incidence from the metallic side for different

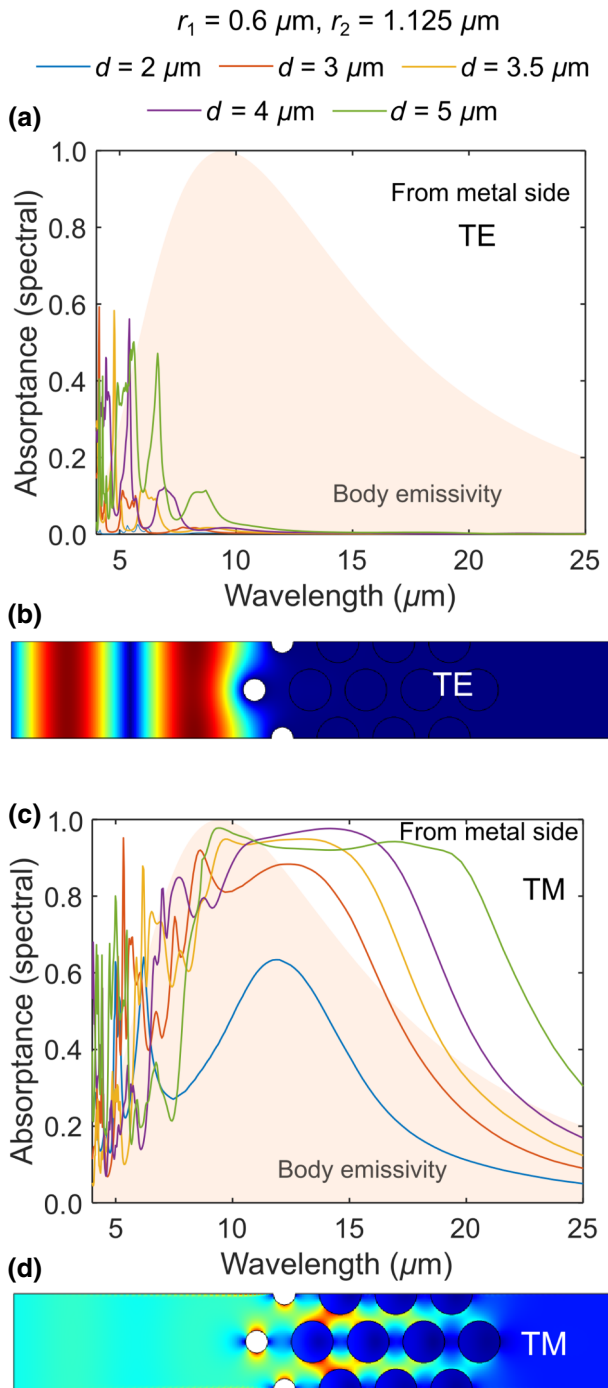


FIG. 6. (a) The TE-mode absorbance of a yarn ($r_1 = 0.6 \mu\text{m}$, $r_2 = 1.125 \mu\text{m}$) for separations d of 2, 3, 3.5, 4, and 5 μm , metal incidence. (b) The electric field norm at $\lambda = 13 \mu\text{m}$ for $d = 3 \mu\text{m}$ TE-mode polarization. (c) The TM-mode absorbance of a yarn ($r_1 = 0.6 \mu\text{m}$, $r_2 = 1.125 \mu\text{m}$) for separations d of 2, 3, 3.5, 4, and 5 μm , metal incidence. (d) The electric field norm at $\lambda = 13 \mu\text{m}$ for $d = 3 \mu\text{m}$, TM-mode polarization.

fiber-separation distances d . In addition, the corresponding field plots of the design with $d = 3 \mu\text{m}$ at a wavelength of 13 μm are displayed accordingly [Figs. 6(b) and 6(d)]. For TE-mode polarization, one can see a complete blockage

of radiative transfer by the metallic fibers due to the plasmonic gap. On the other hand, for TM-mode polarization, radiation is transmitted through the metallic fibers due to the absence of the plasmonic gap.

- [1] H. E. Murdock, D. Gibb, T. André, F. Appavou, A. Brown, B. Epp, B. Kondev, A. McCrone, E. Musolino, and L. Ranalder *et al.*, (2019).
- [2] M. Beerepoot and A. Marmion, *Policies for Renewable Heat: An Integrated Approach*, Tech. Rep. (OECD Publishing, 2012).
- [3] J. D. Hardy and E. F. DuBois, Regulation of heat loss from the human body, *Proc. Natl. Acad. Sci. U.S.A.* **23**, 624 (1937).
- [4] J. K. Tong, X. Huang, S. V. Boriskina, J. Loomis, Y. Xu, and G. Chen, Infrared-transparent visible-opaque fabrics for wearable personal thermal management, *ACS Photonics* **2**, 769 (2015).
- [5] P.-C. Hsu, X. Liu, C. Liu, X. Xie, H. R. Lee, A. J. Welch, T. Zhao, and Y. Cui, Personal thermal management by metallic nanowire-coated textile, *Nano. Lett.* **15**, 365 (2015).
- [6] L. Cai, Y. Peng, J. Xu, C. Zhou, C. Zhou, P. Wu, D. Lin, S. Fan, and Y. Cui, Temperature regulation in colored infrared-transparent polyethylene textiles, *Joule* **3**, 1478 (2019).
- [7] L. Cai, A. Y. Song, P. Wu, P.-C. Hsu, Y. Peng, J. Chen, C. Liu, P. B. Catrysse, Y. Liu, and A. Yang *et al.*, *In situ* click chemistry generation of cyclooxygenase-2 inhibitors, *Nat. Commun.* **8**, 1 (2017).
- [8] P. B. Catrysse, A. Y. Song, and S. Fan, Photonic structure textile design for localized thermal cooling based on a fiber blending scheme, *ACS Photonics* **3**, 2420 (2016).
- [9] Y. Peng, J. Chen, A. Y. Song, P. B. Catrysse, P.-C. Hsu, L. Cai, B. Liu, Y. Zhu, G. Zhou, and D. S. Wu *et al.*, Nanoporous polyethylene microfibrils for large-scale radiative cooling fabric, *Nat. Sustain.* **1**, 105 (2018).
- [10] Z. Li, Z. Xu, Y. Liu, R. Wang, and C. Gao, Multifunctional non-woven fabrics of interfused graphene fibres, *Nat. Commun.* **7**, 1 (2016).
- [11] T. Gao, Z. Yang, C. Chen, Y. Li, K. Fu, J. Dai, E. M. Hitz, H. Xie, B. Liu, and J. Song *et al.*, Three-dimensional printed thermal regulation textiles, *ACS Nano* **11**, 11513 (2017).
- [12] R. Liu, X. Wang, J. Yu, Y. Wang, J. Zhu, and Z. Hu, A novel approach to design nanoporous polyethylene/polyester composite fabric via TIPS for human body cooling, *Macromol. Mater. Eng.* **303**, 1700456 (2018).
- [13] Y. Guo, C. Dun, J. Xu, J. Mu, P. Li, L. Gu, C. Hou, C. A. Hewitt, Q. Zhang, and Y. Li *et al.*, Ultrathin, washable, and large-area graphene papers for personal thermal management, *Small* **13**, 1702645 (2017).
- [14] K. Fu, Z. Yang, Y. Pei, Y. Wang, B. Xu, Y. Wang, B. Yang, and L. Hu, Designing textile architectures for high energy-efficiency human body sweat- and cooling-management, *Adv. Fiber Mater.* **1**, 61 (2019).
- [15] P.-C. Hsu, A. Y. Song, P. B. Catrysse, C. Liu, Y. Peng, J. Xie, S. Fan, and Y. Cui, Radiative human body cooling by nanoporous polyethylene textile, *Science* **353**, 1019 (2016).

- [16] H. Luo, Q. Li, K. Du, Z. Xu, H. Zhu, D. Liu, L. Cai, P. Ghosh, and M. Qiu, An ultra-thin colored textile with simultaneous solar and passive heating abilities, *Nano Energy* **65**, 103998 (2019).
- [17] Q. Liu, J. Huang, J. Zhang, Y. Hong, Y. Wan, Q. Wang, M. Gong, Z. Wu, and C. F. Guo, Thermal, waterproof, breathable, and antibacterial cloth with a nanoporous structure, *ACS Appl. Mater. Interfaces* **10**, 2026 (2018).
- [18] A. Hazarika, B. K. Deka, D. Kim, H. E. Jeong, Y.-B. Park, and H. W. Park, Woven kevlar fiber/polydimethylsiloxane/reduced graphene oxide composite-based personal thermal management with freestanding Cu-Ni core-shell nanowires, *Nano. Lett.* **18**, 6731 (2018).
- [19] K. Wu, L. Yu, C. Lei, J. Huang, D. Liu, Y. Liu, Y. Xie, F. Chen, and Q. Fu, Green production of regenerated cellulose/boron nitride nanosheet textiles for static and dynamic personal cooling, *ACS Appl. Mater. Interfaces* **11**, 40685 (2019).
- [20] Y. Xu, B. Sun, Y. Ling, Q. Fei, Z. Chen, X. Li, P. Guo, N. Jeon, S. Goswami, and Y. Liao *et al.*, Multiscale porous elastomer substrates for multifunctional on-skin electronics with passive-cooling capabilities, *Proc. Natl. Acad. Sci.* **117**, 205 (2020).
- [21] S. Jafar-Zanjani, M. M. Salary, and H. Mosallaei, Metafabrics for thermoregulation and energy-harvesting applications, *ACS Photonics* **4**, 915 (2017).
- [22] L. Cai, A. Y. Song, W. Li, P.-C. Hsu, D. Lin, P. B. Catrysse, Y. Liu, Y. Peng, J. Chen, and H. Wang *et al.*, Spectrally selective nanocomposite textile for outdoor personal cooling, *Adv. Mater.* **30**, 1802152 (2018).
- [23] S. Assaf, M. Boutghatin, Y. Pennec, V. Thomy, A. Korovin, A. Treizebre, M. Carette, A. Akjouj, and B. Djafari-Rouhani, Polymer photonic crystal membrane for thermo-regulating textile, *Sci. Rep.* **10**, 1 (2020).
- [24] M. Boutghatin, S. Assaf, Y. Pennec, M. Carette, V. Thomy, A. Akjouj, and B. Djafari Rouhani, Impact of SiO₂ particles in polyethylene textile membrane for indoor personal heating, *Nanomaterials* **10**, 1968 (2020).
- [25] X. A. Zhang, S. Yu, B. Xu, M. Li, Z. Peng, Y. Wang, S. Deng, X. Wu, Z. Wu, and M. Ouyang *et al.*, Dynamic gating of infrared radiation in a textile, *Science* **363**, 619 (2019).
- [26] P.-C. Hsu, C. Liu, A. Y. Song, Z. Zhang, Y. Peng, J. Xie, K. Liu, C.-L. Wu, P. B. Catrysse, and L. Cai *et al.*, A dual-mode textile for human body radiative heating and cooling, *Sci. Adv.* **3**, e1700895 (2017).
- [27] E. M. Leung, M. C. Escobar, G. T. Stiubianu, S. R. Jim, A. L. Vyatskikh, Z. Feng, N. Garner, P. Patel, K. L. Naughton, and M. Follador *et al.*, A dynamic thermoregulatory material inspired by squid skin, *Nat. Commun.* **10**, 1 (2019).
- [28] M. G. Abebe, G. Rosolen, E. Khouzakoun, J. Odent, J.-M. Raquez, S. Desprez, and B. Maes, Dynamic Thermal-Regulating Textiles with Metallic Fibers Based on a Switchable Transmittance, *Phys. Rev. Appl.* **14**, 044030 (2020).
- [29] H. Luo, Y. Zhu, Z. Xu, Y. Hong, P. Ghosh, S. Kaur, M. Wu, C. Yang, M. Qiu, and Q. Li, Outdoor personal thermal management with simultaneous electricity generation, *Nano. Lett.* **21**, 3879 (2021).
- [30] B. Gu, K. Liang, T. Zhang, X. Yue, F. Qiu, D. Yang, and M. Chen, Fabrication of sandwich-structured cellulose composite membranes for switchable infrared radiation, *Cellulose* **26**, 8745 (2019).
- [31] B. Gu, K. Liang, T. Zhang, F. Qiu, D. Yang, and M. Chen, Multifunctional laminated membranes with adjustable infrared radiation for personal thermal management applications, *Cellulose* **27**, 8471 (2020).
- [32] B. Gu, M. He, D. Yang, X. Yue, F. Qiu, T. Zhang, and M. Chen, Wearable Janus MnO₂ hybrid membranes for thermal comfort management applications, *Appl. Surf. Sci.* **509**, 145170 (2020).
- [33] B. Dai, K. Li, L. Shi, X. Wan, X. Liu, F. Zhang, L. Jiang, and S. Wang, Bioinspired Janus textile with conical micropores for human body moisture and thermal management, *Adv. Mater.* **31**, 1904113 (2019).
- [34] B. Gu, H. Zhou, Z. Zhang, T. Zhang, M. Chen, F. Qiu, and D. Yang, Cellulose-based hybrid membrane with functional integration for personal thermal management applications, *Appl. Surf. Sci.* **535**, 147670 (2021).
- [35] Y. Wang, *Composite materials with self regulated infrared emissivity and environment responsive fibers*, Tech. Rep. Pub. No.: US 2016/0376747 A1 (United States Patent and Trademark Office, 2016).
- [36] B. W. Olesen, olesen1982thermal, *Tech. Rev.* **2**, 3 (1982).
- [37] B. W. Olesen and K. Parsons, Introduction to thermal comfort standards and to the proposed new version of EN ISO 7730, *Energy. Build.* **34**, 537 (2002).
- [38] J. I. Larruquert, A. P. Pérez-Marín, S. García-Cortés, L. Rodríguez-de Marcos, J. A. Aznárez, and J. A. Méndez, Self-consistent optical constants of SiC thin films, *JOSA A* **28**, 2340 (2011).
- [39] See the Supplemental Material at <http://link.aps.org/supplemental/10.1103/PhysRevApplied.16.054013> for heat-transfer analysis, the thermal-circuit analogy of semitransparent and opaque fabrics, thermal constants, crossed-wire-configuration geometry, the spectral absorptance for a disordered array, and the spectral absorptance comparison between the crossed-wire (3D-simulation) and noncrossed-wire (2D-simulation) configurations.
- [40] W. Wei, Y. Zhu, Q. Li, Z. Cheng, Y. Yao, Q. Zhao, P. Zhang, X. Liu, Z. Chen, and F. Xu *et al.*, An Al₂O₃-cellulose acetate-coated textile for human body cooling, *Solar Energy Mater. Solar Cells* **211**, 110525 (2020).
- [41] Y. Yang, X. Bao, Q. Wang, P. Wang, M. Zhou, and Y. Yu, Thermo-responsive cotton fabric prepared by enzyme-initiated “graft from” polymerization for moisture/thermal management, *Cellulose* **28**, 1795 (2021).
- [42] T. Duolikun, N. Ghazali, B. F. Leo, H. V. Lee, C. W. Lai, and M. R. B. Johan, Asymmetric cellulosic membranes: Current and future aspects, *Symmetry* **12**, 1160 (2020).
- [43] Y. Cengel and T. M. Heat, *A Practical Approach* (McGraw-Hill, New York, NY, USA, 2003).
- [44] O. Takayama and M. Cada, Two-dimensional metallo-dielectric photonic crystals embedded in anodic porous alumina for optical wavelengths, *Appl. Phys. Lett.* **85**, 1311 (2004).
- [45] V. Kuzmiak, A. Maradudin, and F. Pincemin, Photonic band structures of two-dimensional systems containing metallic components, *Phys. Rev. B* **50**, 16835 (1994).

- [46] M. M. Sigalas, C. T. Chan, K. Ho, and C. M. Soukoulis, Metallic photonic band-gap materials, *Phys. Rev. B* **52**, 11744 (1995).
- [47] V. Kuzmiak and A. Maradudin, Photonic band structures of one- and two-dimensional periodic systems with metallic components in the presence of dissipation, *Phys. Rev. B* **55**, 7427 (1997).
- [48] M. Shaban, A. M. Ahmed, E. Abdel-Rahman, and H. Hamdy, Ror2 signaling regulates Golgi structure and transport through IFT20 for tumor invasiveness, *Sci. Rep.* **7**, 1 (2017).
- [49] J. D. McCann, *Build the Perfect Survival Kit* (Penguin, New York, 2013).
- [50] D. Ding, T. Tang, G. Song, and A. McDonald, Characterizing the performance of a single-layer fabric system through a heat and mass transfer model—part I: Heat and mass transfer model, *Textile Res. J.* **81**, 398 (2011).